Journal of Molecular Liquids 407 (2024) 125154

Contents lists available at ScienceDirect

Journal of Molecular Liquids

journal homepage: www.elsevier.com/locate/molliq

Molecular dynamics study of the temperature dependence of viscosity and thermal conductivity of molten salts FLiNaK and FLiNaK with LaF_3 or NdF_3

Ksenia Abramova [a,b,*], Alexander Galashev [a,b], Oksana Rakhmanova [a,b], Konstantin Katin [c], Mikhail Maslov [c]

[a] Institute of High-Temperature Electrochemistry, Ural Branch of Russian Academy of Sciences, Academicheskaya Str., 20, Yekaterinburg 620990, Russia
[b] Ural Federal University named after the first President of Russia B.N. Yeltsin, Mira Str., 19, Yekaterinburg 620002, Russia
[c] National Research Nuclear University MIPhI, Kashirskoe Rd., 31, Moscow 115409 Russia

ARTICLE INFO

Keywords:
Connectivity
Molecular dynamic
Molten salt
Viscosity
Thermal conductivity

ABSTRACT

In this work, the temperature dependence of the viscosity and thermal conductivity of molten systems FLiNaK and FLiNaK-MeF_3 (Me = La, Nd) was studied using the molecular dynamics method with Born-Mayer-Huggins potential. The dependencies were obtained in the temperature range of $800 < T < 1020$ K, as well as for the concentration of lanthanide fluoride additives up to 15 mol.%. The temperature behavior of these kinetic properties is explained based on an MD model of dynamic ionic connectivity. The main contribution to the connectivity of pure FLiNaK ions is made by Li-F ion pairs, and in the presence of LaF_3 and NdF_3 dissolved in the salt mixture, the connectivity in the system is supplemented by ion pairs formed by lanthanides with fluorine. Both viscosity and thermal conductivity decrease with increasing temperature and rise when lanthanide trifluorides are added to the molten salt.

1. Introduction

Molten salt reactor (MSR) is a type of reactor that combine aspects of both nuclear and chemical reactors [1]. The fuel for such a reactor is nuclear fuel dissolved in the molten salt. Such a melt is either pumped through the primary circuit or is in a slightly changing state in pipes located inside the core. MSRs have increased passive safety, fuel cycle flexibility, and provide an alternative economic use of nuclear energy. Due to their suitability for industrial production of heat and isotopes, the development of improved MSRs is considered to be a promising area of study [2]. However, the multiphysics behavior of MSR requires a wide range of studies, such as neutronics, thermohydraulics, coolant chemistry, etc. [3]. Fluid flow and thermal properties of the molten salt are important characteristics that largely determine the performance of MSR. FLiNaK (46.5 LiF–11.5 NaF–42 KF mol.%) and FLiBe (66 LiF-34BeF_2 mol.%) are among the most well-known and proven coolants used in MSR [4]. Predicting the behavior of molten salts when they are saturated with fission products of radioactive fuel is an important scientific and practical task.

Traditionally, computer simulation methods are used to study the physicochemical properties of melts. The high aggressiveness of the environment, high temperatures, inaccessibility and radioactivity of some samples make it impossible to execute a real experiment [5–7]. At the same time, to optimize the operation of MSR, it is important to develop a reliable predictive model that can properly describe the behavior of molten systems both when the composition varies and when the external parameters of the reactor operation change. Accurate accounting of flow regimes and heat transfer of molten salts can be made based on data on transport coefficients.

To design pumps that move molten salt around an MSR or concentrated solar power plant, it is necessary to know the flow behavior of the molten salt, which is described by its viscosity. The physical meaning of fluid viscosity is to quantify its resistance to flow and ability to dissipate momentum. Typically, shear viscosity is defined as the ratio of shear stress divided to the velocity gradient. Viscosity of solids and liquids depends on the chemical composition of the material and determines the relaxation time, i.e. the time required to achieve stabilized material properties. Temperature has a strong influence on viscosity. The activation energy for flow decreases with increasing temperature, and the viscosity decreases. There are various model approaches for the microscopic description of viscosity behavior [8]. For example, according to the valence-configuration theory, viscous flow is an activated switching

* Corresponding author.
E-mail address: abramova@ihte.ru (K. Abramova).

https://doi.org/10.1016/j.molliq.2024.125154
Received 30 January 2024; Received in revised form 8 May 2024; Accepted 28 May 2024
Available online 29 May 2024

of valence bonds between atoms [9].

Thermal conductivity is a key characteristic that plays a significant role in the selection of salts both as a heat transfer fluid and for their application within the reactor core. Experimental measurement of the thermal conductivity of high-temperature molten salts is a challenging task, as the results are extremely sensitive to both the measurement method and the composition of the salt [10]. The values obtained by different authors show a large scatter and ambiguous temperature dependence (Fig. 1) [11–17]. In addition to the purity of the investigated salt composition, the main reasons for discrepancies in the literature data are attributed to thermal losses during the measurement process.

The thermal conductivity of solid crystalline is determined by the collective vibrations of the lattice, i.e. phonons. In the case of amorphous solids, the picture of heat transfer becomes more complicated. Along with the phonon-like mechanism, there may be other ways of energy transfer, for example, heat transfer using delocalized modes that have a diffusion character of propagation [18,19]. In molten salts, a significant part of the energy transfer is carried out due to the random walk of categorical oscillations [20], i.e., vibrations determined by a certain type of ions. Such vibrations mainly appear due to the bonds that are formed by the smallest, lightest and most mobile positive ions, as well as high valence cations with the negative ions present in the melt. Thus, thermal conductivity in molten salts is related to the microstructure of the melts. Consequently, by modifying the structure of the molten salt, it is possible to control its thermal conductivity.

The increase in the viscosity of the system is largely due to the presence of a dynamic network of bonds between ions, or dynamic ionic connectivity. This bonding is determined by the strong Coulombic interaction between closely spaced ions of opposite charges. The dynamic nature of bonding is that it changes rapidly over time, i.e. due to the rapid movement of ions, bonds are constantly broken and recreated.

It can be noted, that dynamic viscosity and thermal conductivity of a liquid are not independent characteristics. Their connection is evident from the following example. If the temperature of a flowing fluid increases, its viscosity decreases. A decrease in viscosity leads to an increase in the fluid flow rate and an enhanced rate of heat transfer at the wall, affecting thermal conductivity.

In this study, the behavior of viscosity and thermal conductivity of pure FLiNaK molten salt is investigated using classical equilibrium molecular dynamics (MD). Additionally, the characterization of the changes in kinetic properties upon the addition of the rare earth element fluorides to the molten salt is studied. Thus, the focus of this work is the investigation of the properties of the system FLiNaK + MeF_3 (Me = La^{3+}, Nd^{3+}) in the wide temperature range.

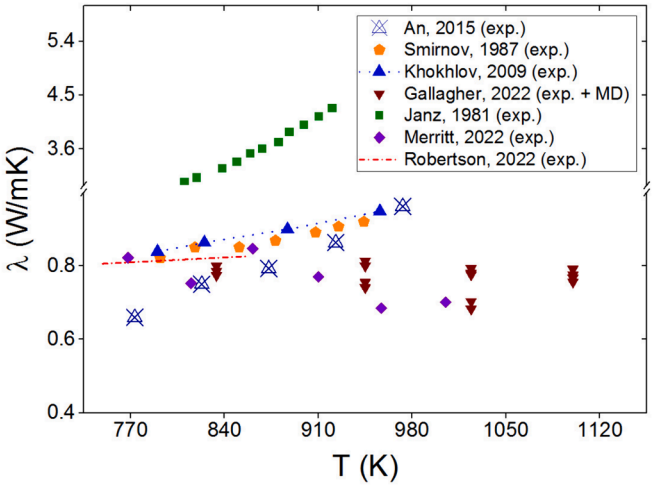

Fig. 1. The temperature dependence of thermal conductivity of pure FLiNaK system obtained by various authors: X.-H. An [11], M.V. Smirnov [12], V.A. Khohlov [13], R. Gallagher [14], G.J. Janz [15], B. Merritt [16], S.G. Robertson [17].

2. Molecular dynamics model

The LiF-NaF-KF (FLiNaK) system consisted of 20,000 particles. The number of particles in the melt corresponded to the eutectic composition of LiF-NaF-KF (46.5–11.5–42 mol. %): LiF (9300 ions), NaF (2300 ions), KF (8400 ions). The molar ratio of the components was calculated in accordance with the following definition: N_i/N_{all} (where N_i is the number of atoms of the individual salt and N_{all} is the total number of atoms in the molten system). The size of the simulation cell was 12.1 × 3.4 × 11.7 nm. Temperature and pressure control in the model were carried out using the standard procedure within the framework of the Nosé-Hoover dynamics approach [21].

The Born-Mayer-Huggins (BMH) potential in the form (1) without taking into account the polarization effects [22] was used to describe the interatomic interactions.

$$U(r) = \frac{q_i q_j}{r_{ij}} + A \bullet exp\left(\frac{\sigma - r}{\rho}\right) - \frac{C}{r^6} + \frac{D}{r^8} \quad (1)$$

The first term describes the Coulombic interaction between ions in the molten system, where q is the ionic charge, r_{ij} is the interatomic distance between i-j ions. The second term is the short-range repulsive interaction, where A is the Pauling factor, σ is the ionic radius of i charge particle and ρ is a bond "hardness" parameter. The last two terms correspond to dipole–dipole and dipole-quadrupole dispersion interactions, where C and D are the dispersion parameters.

The interaction parameters between the ions of the FLiNaK melt with additions of MeF_3 (Me = La^{3+}, Nd^{3+}) were determined in separate calculations using Density Functional Theory (DFT) within the Generalized Gradient Approximation (GGA) and employing scalar relativistic pseudopotentials. The obtained parameters are presented in Table 1. The procedure for calculating the parameters of the BMH potential for pairs of ions Me-Me, Me-FLiNaK (Me = La^{3+}, Nd^{3+}) is discussed in more detail in the Supplementary Material 1 section.

It should be noted that the polarization model, when describing the behavior of molten halide salts – ionic melts, is a common approach and increases the accuracy of calculations [14,23]. In the present work, it was of interest to study the effect of adding lanthanide fluorides LaF_3 and NdF_3 on the behavior of the FLiNaK melt. In this case, the introduction of expensive (in terms of computing resources) polarization would significantly reduce the speed of calculations and the dimensions of the system available for modeling. Since the calculation of transport coefficients is associated with the calculation of autocorrelation functions depending on heterogeneous collective coordinates, we opted for a simplified model that does not take the polarization into account.

Similar to the work [24], the simulation consisted of two steps. Firstly, the crystals of LiF, NaF, KF and MeF_3 (Me = La^{3+}, Nd^{3+}) were melted in the NVT ensemble, with control measures taken to ensure good mixing (by visual layer-by-layer observation of the structure in the model and by analyzing partial radial distribution functions). The obtained equilibrated melt was the result of this step. In the second stage, under the conditions of the NPT and NVE ensembles, the geometric optimization, relaxation, and calculation of physicochemical properties were performed. Fig. 2 shows the FLiNaK-LaF_3 (10 mol.%) system after melting and relaxation (left), as well as the radial distribution functions $g(r)$ of the melt components, along with the $g(r)$ obtained in the work [6] for the pure FLiNaK melt (right). In the bottom right in Fig. 2 the behavior of pressure and specific energy (potential and total) of the molten salt mixture during the relaxation process of the system in the NPT ensemble is shown.

During the melting stage, the system was overheated to 3000 K for 0.5 ns in the NVT ensemble. Subsequently, the system was cooled to the operating temperature within the range of 800 ≤ T ≤ 1020 K over a

Table 1
Parameters for interaction of La^{3+} and Nd^{3+} with the components of FLiNaK molten salt.

Lanthanum	*A*, eV	*ρ*, Å	*σ*, Å	Neodymium	*A*, eV	*ρ*, Å	*σ*, Å
La^{3+} – La^{3+}	1.158	0.151	2.06	Nd^{3+} – Nd^{3+}	0.723	0.117	1.96
La^{3+} – F^{-}	2.541	0.33	2.36	Nd^{3+} – F^{-}	1.634	0.3328	2.31
La^{3+} – Li^{+}	0.046	0.141	1.79	Nd^{3+} – Li^{+}	0.012	0.110	1.74
La^{3+} – Na^{+}	0.106	0.154	2.05	Nd^{3+} – Na^{+}	0.028	0.121	2.00
La^{3+} – K^{+}	0.078	0.174	2.41	Nd^{3+} – K^{+}	0.032	0.146	2.36

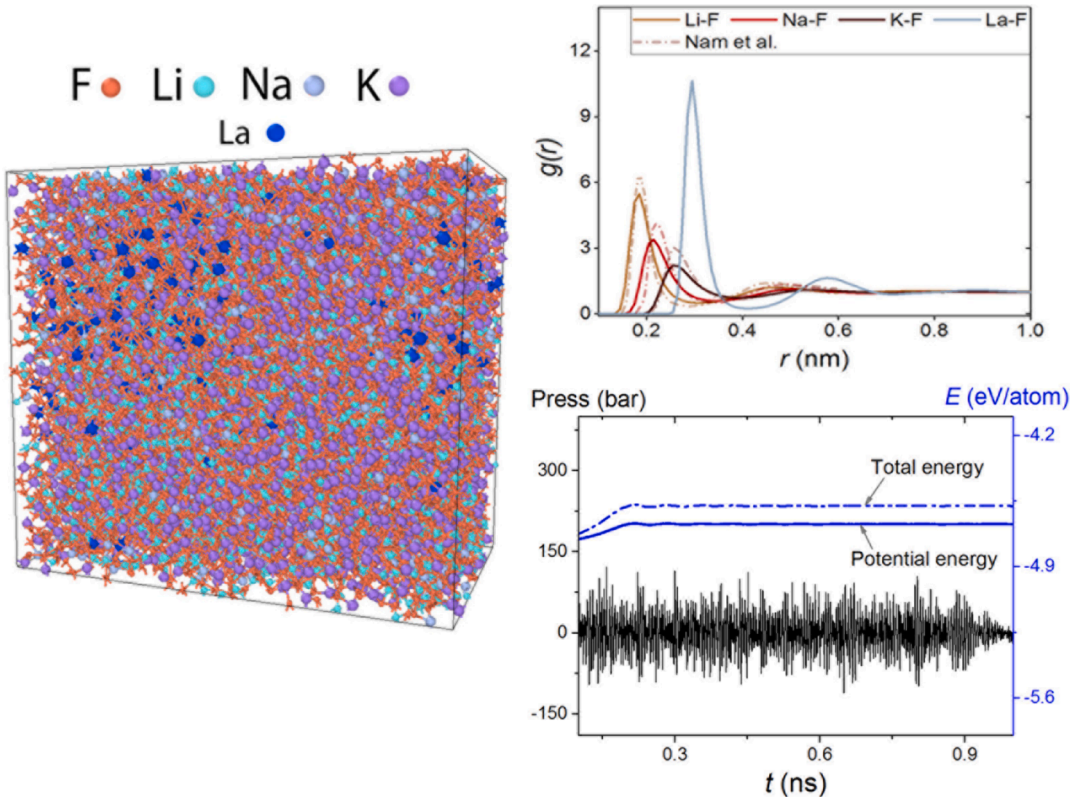

Fig. 2. The general view of the FLiNaK + LaF_3 (10 mol.%) system obtained by the final moment of the melting process (on the left); on the right, the radial distribution functions of the melt components are presented; g(r) values obtained for pure FLiNaK in the work [6] are indicated by dash-dot lines; the fluctuations in pressure and specific energy (E/atom) during the relaxation of the system in the NPT ensemble are shown below.

duration of 1 ns. At the operating temperature, the melt was adjusted to the experimental density under constant pressure conditions (in the NPT ensemble). Once the system reached equilibrium, the dynamic viscosity (η) and thermal conductivity (λ) calculations were executed. Several calculations were performed for the thermal conductivity at different melt densities (at elevated pressures of $P = 10{,}000$, 15,000, and 20,000 bar) to determine the degree of influence of temperature and density on the value of λ.

All calculations were performed with the use of the open source program code for MD simulation LAMMPS [25] on a URAN cluster-type hybrid computer at the N.N. Krasovskii Institute of Mathematics and Mechanics UB RAS. We used Ovito version 3.0.0 [26] for the visualization of the molten salt structure.

3. Defining a dynamic network of ionic bonds in simulated systems

Both propagative ("propagons") and diffusive components contribute to the thermal conductivity of disordered materials [27]. The term "propagons" refers to propagating phonons with a certain vector of direction of motion. Diffusion components are both atoms characterized exclusively by translational motion and "diffusons", i.e. vibrational modes with a wandering direction of propagation. "Propagons" (phonons) can be characterized by the mean free path l_p, which is related to thermal conductivity λ by the expression

$$\lambda_p = \frac{1}{3} C_v v_s l_p \tag{2}$$

where λ_p is the phonon component of thermal conductivity, is the volumetric heat capacity and v_s is the speed of sound.

In the case of molten salt mixtures, as well as for quartz glass melts, the contribution to the thermal conductivity from the diffusive component is insignificant (~5%), and the main contribution to λ is made by the propagating vibration mode (i.e., phonons) [27,28]. The high-frequency collective excitations (optical phonon-like modes), caused by fast charge fluctuations, can propagate in molten salt mixtures along with acoustic "propagons" typical of other disordered systems [29].

Interatomic distances increase with rising temperature, reducing the heat transfer of "propagons", and the thermal conductivity of typical liquids decreases. It is not possible to explain the positive temperature trend in thermal conductivity, often observed in fluoride salt liquid mixtures, solely by typical "propagons" and convective heat transfer [17]. Most likely, typical "propagons" and "diffusons" in such a system do not contribute to the abnormal temperature changes in thermal

conductivity. In this case, optical "propagons" propagating as electromagnetic waves must be included in the consideration.

We establish categorical collective fluctuations in the model based on the composition of the molten salt. This arises from the fact that ions with similar electrical charges, but varying in size and mass, exhibit different behavior within the molten salt. In the molten salt considered here, there are strong electrostatic interactions between cations and anions, which create the conditions for the formation of complex nanostructures. To construct and further analyze the network of short-term bonds formed in the melt between ions at a certain time step, we introduced a characteristic – connectivity. In the melt, such a bond acts as an electron donor from the F^- ion to the Li^+ ion. Essentially, the bond is formed as a result of deformation of the electron shells of colliding ions. Chemical interactions also cause changes in the charge density distribution. Although in the molten salt with exclusively monovalent ions, cations and anions alternate evenly, short-lived dipole moments are formed only for cation–anion pairs with the shortest interionic distances. The presence of an electromagnetic field in the real molten salt, due to the dynamically formed network of dipole moments, leads to the propagation of spontaneous electromagnetic waves in the medium. In this interaction, part of the internal energy of the ions is carried away. The amount and intensity of the removing internal energy will be determined by internal friction in the medium. This approach can give a concept of the nature of heat and mass transfer in the melt; the essence of this effect is discussed in more detail in the Supplementary Material 2 section.

Since the interionic bond is established through an electron, i.e. a very small particle, and due to the spherical symmetry of colliding ions, the angular dependence of the emerging bond disappears. In this case, the only bond parameter is the distance between the ions forming a pair. Understanding the basic interactions and structures is important for the use of fluoride molten salts in chemical and related fields.

To determine the connectivity in the melt at every time step, we utilized a custom program to track the quantity of bonds with certain bond lengths forming between the ions in the system. First of all, when investigating the FLiNaK and FLiNaK + MeF_3 systems (Me = La^{3+}, Nd^{3+}), our focus was on studying the number of Li^+ bonds with F^-. This is due to the fact that Li^+ ions are the most dominant positive ions in these systems. In addition, these are the most dynamic ions, making them more responsive to variations in external conditions, i.e. temperature and density. Finally, Li^+ ions form the strongest bonds with F^- ions, characterized by the shortest bond length. Most likely, it is precisely such connections that can lead to the emergence of categorical collective fluctuations in the molten salt under examination. The program used to determine the connectivity of ions in the system analyzed the coordinates of all ions in the system, recorded at equal time intervals (100 ps). Using this program, it was found that at all temperatures and densities considered, bonds with a length not exceeding 0.2 nm were predominantly formed between Li^+ and F^- ions. The remaining positive ions accounted for less than 0.1 % of these bonds with F^- ions. Thus, the value of 0.2 nm served as a connectivity parameter in the models of the molten salt melts under investigation. The functionality of the connectivity program is based on the choice of distances between all (or some specific) positive and all negative ions of the system, which satisfy the condition $r \leq 0.2$ nm or $r \leq 0.27$ nm for subsystems containing cations with high valence. When saving a list of such distances, the numbers of the ions between which these shorter distances were established were simultaneously recorded. Both threshold distances (0.2 and 0.27 nm fall within the range between the first maximum and minimum of the corresponding partial radial distribution function. The minimum distance between Li^+ and F^- ions in molten salts containing lanthanide trifluorides was ~ 0.14–0.17 nm, and between Nd^{3+} (La^{3+}) and F^- ions that was 0.203–0.207 nm.

After such complete processing of the entire configuration, based on the saved numbers of the selected ions, an analysis of the connectivity of the selected charged particles was executed. A necessary condition for obtaining a coherent structure (i.e. network) was the presence of at least two bonds (close neighbors) for each selected ion. In other words, the number of each bound ion had to appear in the list of numbers at least twice. To determine the numbers of different ions forming the network, it was enough to perform another reduction in the list of ions, ensuring that each ion forming the network appeared only once. As a result, we received a representation of the connectivity in the system, i.e., the coordinates of the ions forming a network of bonds. In addition, the minimum and maximum (typically 0.2 nm) distances in the resulting network of bonds were determined. The number of ions (both positive and negative) forming a connected network could be visually represented in relative units or percentages relative to the total number of ions in the system.

4. Molecular dynamics calculation of physical–chemical properties of molten salts

In this study, viscosity and thermal conductivity are computed using the Green-Kubo formalism [30] by the equilibrium molecular dynamic (EMD) approach. The dynamic viscosity is calculated as the time integral of the autocorrelation function of the off-diagonal elements of the pressure tensor in a fully equilibrated system:

$$\eta = \frac{V}{k_B T}\int_0^\infty \langle \boldsymbol{P}_{\alpha\beta}(0) \bullet \boldsymbol{P}_{\alpha\beta}(t)\rangle dt \tag{3}$$

where $\boldsymbol{P}_{\alpha\beta}$ are the off-diagonal components of the pressure tensor, <… > is an average over the particles ensemble, $k_B = 1.381{\cdot}10^{-23}$ J/K is the Boltzmann constant, V is the system volume, T is the temperature.

The thermal conductivity of the FLiNaK, and FLiNaK + MeF_3 systems is calculated according to the equation:

$$\lambda = \frac{1}{3Vk_B T^2}\int_0^\infty \langle \boldsymbol{j}(0) \bullet \boldsymbol{j}(t)\rangle dt \tag{4}$$

where the subintegral expression $\langle \boldsymbol{j}(0) \bullet \boldsymbol{j}(t)\rangle$ is the flow autocorrelation function, and the heat flow is defined as

$$j = \frac{1}{2}\sum_{i=1}^{N}\left[m_i v_i^2 + \sum_{j\neq i}^{N} u(r_{ij})\right] \bullet v_i + \frac{1}{2}\sum_{i=1}^{N}\sum_{j\neq i}^{N}(r_{ij}F_{ij}) \bullet v_i \tag{5}$$

where, the first term describes the flow of total energy, while the second term represents the flow associated with the forces (F_{ij}) acting between atoms, N is the number of ions in the system.

As noted in work [31], devoted to the EMD calculation of the thermal conductivity of the NaCl melt at a temperature of 1300 K, when determining the transport coefficients, many factors can influence the obtained values. In particular, the authors discuss that when calculating thermal conductivity, the error in calculating energy and force flows (the integrand in the expressions (3), 4)) is most significantly influenced by: the parameters for Ewald sums; the number of time steps at which flows are calculated; as well as the presence of an uncompensated momentum in the system (the presence of an additive to the speed in a certain direction). Based on the data [31,32], in our work, the conditions for modeling transport processes met the following criteria: the time step used for numerical integration of the equations of motion was 0.1 fs. The Coulombic interactions between ions were calculated based on the conventional PPPM (Particle-Particle Particle-Mesh) method [33] using periodic boundary conditions. The calculation of energy and force flows was carried out for isolated systems under the NVE ensemble condition; such flows were caused exclusively by internal mechanisms of heat and mass transfer in melts. The calculation of correlation functions for the systems FLiNaK, FLiNaK + MeF_3 (Me = La^{3+}, Nd^{3+}) was carried out for temperatures in the range of 750 < T < 900 K on a time interval of 500000Δt, which corresponded to 500 ps. Fig. 3 shows the convergence of the normalized heat current autocorrelation function (HCACF) over a time interval of 300 ps for temperatures 750, 800 and 850 K. The

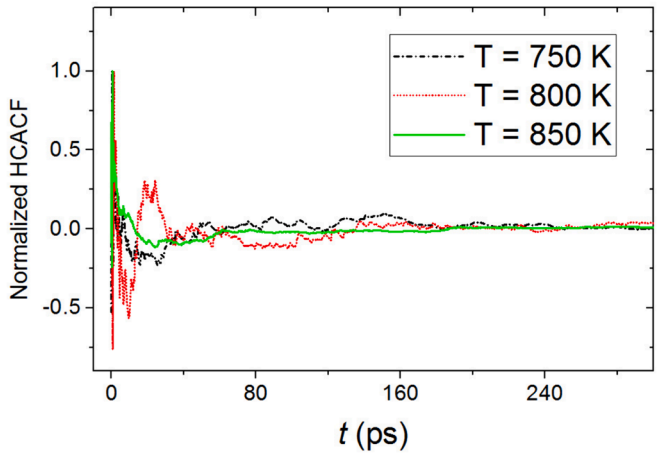

Fig. 3. Normalized heat current autocorrelation function (HCACF) over the time moment of 300 ps of simulation under the NVE ensemble conditions for the pure FLiNaK system; the data presented for $T = 750$, 800 and 850 K.

normalized HCACF was calculated in accordance with the definition $\frac{\langle j(t) \bullet j(0) \rangle}{\langle j(0)^2 \rangle}$, where the autocorrelation function of the heat current is in the numerator and the denominator – is the maximum value of the function at $t = 0$ ps.

5. Calculation results

5.1. Dynamic network of connections in simulated systems

The degree of network development, namely the number of bonds not exceeding 0.2 nm in length between positive and negative ions, and how it changes with temperature and due to the addition of LaF_3 (10 mol.%) to FLiNaK is depicted in Fig. 4. In pure FLiNaK, on average from 3.0 to 6.1 % of all ions are involved in the formation of such bonds. With increasing temperature, the proportion of bonds under consideration and the number of ions forming them decreases, except for temperatures below 850 K. This pattern is observed both in pure FLiNaK and in molten salt mixtures, i.e., FLiNaK with LaF_3 and NdF_3 additives (Fig. 4 only displays data with the addition of LaF_3). In all cases considered, introducing 10 mol.% of LaF_3 to FLiNaK leads to an increase in the considered molten salt connectivity. Note that both in pure FLiNaK and in the presence of LaF_3 or NdF_3 additives, the considered dynamic connectivity of ions is not stable. Moreover, over time it can completely disappear and reappear. A decrease in the connectivity of the system with rising temperature indicates a negative temperature trend in the value of viscosity (η). The decrease in viscosity in this temperature range for pure FLiNaK was 55.2 %, and for FLiNaK + 10 mol.% LaF_3 it was 70.4 %. The concentration trend of viscosity has the opposite sign. The increase in viscosity is mainly due to a sharp increase in the density of the system when lanthanide fluorides are dissolved in FLiNaK. Thus, the dissolution of LaF_3 in FLiNaK at a temperature of 800 K led to an increase in the density of the system by 24.2 %.

Fig. 5 shows the nodes of the considered bond network in pure FLiNaK at a temperature of 1000 K. The configurations of the ions forming the network refers to the time instants of (a) 1.7 and (b) 1.8 ns. It is noteworthy that the network of bonds does not cover the entire small volume of the MD cell, but is localized in some relatively part of it. Moreover, the location of the area in which the network of bonds is located changes over time. In other words, a network of bonds can disappear in one area of space and appear in another area. The existence in the system of fragments of a dynamic network of bonds appearing and disappearing in different parts of the system can serve as an additional factor in increasing the thermal conductivity of the system, because its presence means the existence of optical "propagons" and "diffusons". In this regard, it can be expected that a simulated molten salt system with

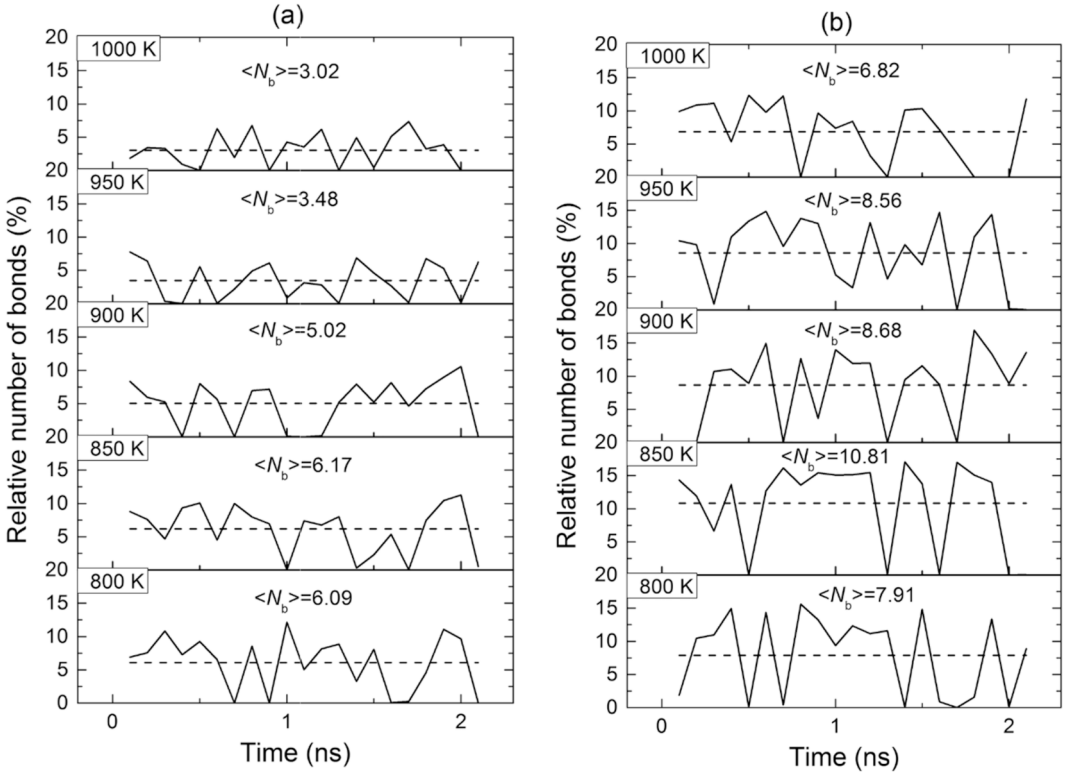

Fig. 4. Relative number of bonded ions with a bond length not exceeding 0.2 nm between positive and negative ions in the systems: (a) FLiNaK, (b) FLiNaK + 10 mol. % LaF_3; the dotted line and numbers show the average N_b/N values; the temperature corresponding to the resulting dependence is shown in the upper left corner of each part of the figure.

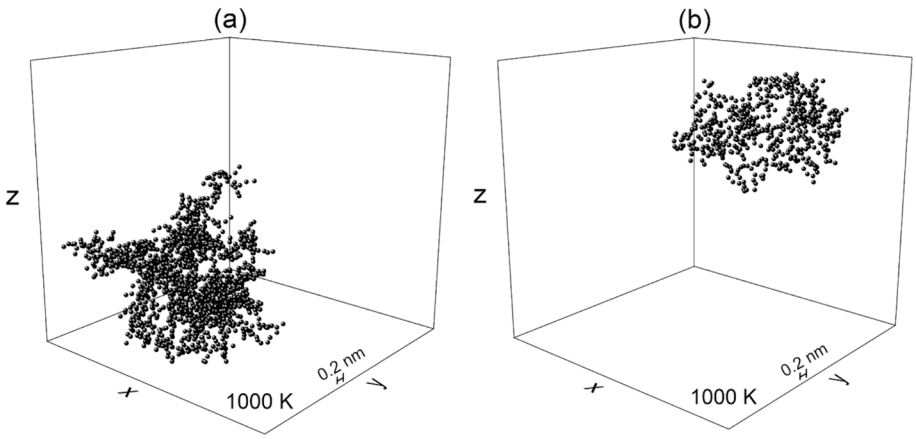

Fig. 5. Nodes of the dynamic bond network with bond lengths not exceeding 0.2 nm between positive and negative ions in the FLiNaK system at a temperature of 1000 K: (a) at a time of 1.7 ns, (b) at a time of 1.8 ns.

LaF_3 and NdF_3 inclusions will have higher thermal conductivity than a pure FLiNaK molten salt.

The addition of lanthanide tetrafluoride leads to the appearance of additional F^- ions in the system, with the help of which the dynamic connectivity expands with a threshold bond length value of 0.2 nm. However, the trivalent ion itself (La^{3+} or Nd^{3+}) can create stronger bonds with the F^- ion in the molten salt than any of the monovalent cations can. The presence of such bonds, leading to the appearance of associates in the system, is shown in [24]. At a sufficiently high concentration of trivalent cations in the system (as in the case of 15 mol.% NdF_3) and a large number of anions, such as F^-, networks of bonds from ions such as Nd^{3+} (La^{3+}) and F^- can also be formed in the system. This is also facilitated by the situation when trivalent ions are crowded in some place in the volume of the system, i.e. their distribution over the volume is not completely uniform. This new categorical bond network will have an effect on the kinetic properties of the system similar to the bond network with a threshold bond length value of 0.2 nm.

The placement of Nd^{3+} ions in the FLiNaK + 15 mol.% NdF_3 system at the end of the MD calculation at temperatures of 850 K and 1020 K is shown in Fig. 6. As can be seen from the figure, in both cases, the placement of trivalent cations throughout the volume of the MD cell is not uniform. In the center of the MD cell, a concentration of Nd^{3+} ions is observed. Consequently, in the vicinity of the center of the MD cell, one should expect the appearance of a network of bonds formed by Nd^{3+} and F^- ions.

The nodes of the dynamic bond networks between Nd^{3+} and F^- ions for the configurations are shown in Fig. 7. The figure shows networks with the maximum number of bonds observed throughout the MD calculation formed by Nd^{3+} and F^- ions. The number of nodes in the network varied from 3 to 1098 at a temperature of 850 K and from 5 to 853 at 1020 K. Since heavy ions (Nd^{3+}) are displaced by insignificant distances during MD calculations, these new categorical networks are located approximately in the same place at different temperatures. Of course, the shape and number of bonds in these networks at temperatures of 850 K and 1020 K are significantly different. A distinctive feature of the bond networks formed by Nd^{3+} and F^- ions with a threshold bond length value of 0.27 nm, as compared to the networks formed by Li^+ and F^- ions with a threshold bond length value of 0.2 nm, is the stable location of the former and the time-varying localization of the latter.

Fig. 8 shows the temperature dependence of the average dynamic connectivity of the FLiNaK and FLiNaK + 15 mol.% NdF_3 systems, obtained with a threshold bond length value of 0.2 nm for connectivity, as well as for the latter system with combined or total connectivity. The additional connectivity due to the presence of trivalent Nd^{3+} (as well as La^{3+}) ions was established only for the component introduced into FLiNaK. In this case, a threshold bond length value of 0.27 nm for establishing Nd-F bonds was used. The validity of the chosen threshold bond length values in determining connectivity is discussed in the Discussion section.

5.2. Viscosity of the FLiNaK + LaF_3 molten system

Initially, in the MD model, the viscosity of the pure FLiNaK system was calculated, and the obtained data were compared with the results of various authors. In the wide temperature range of 750 < T < 1020 K, the

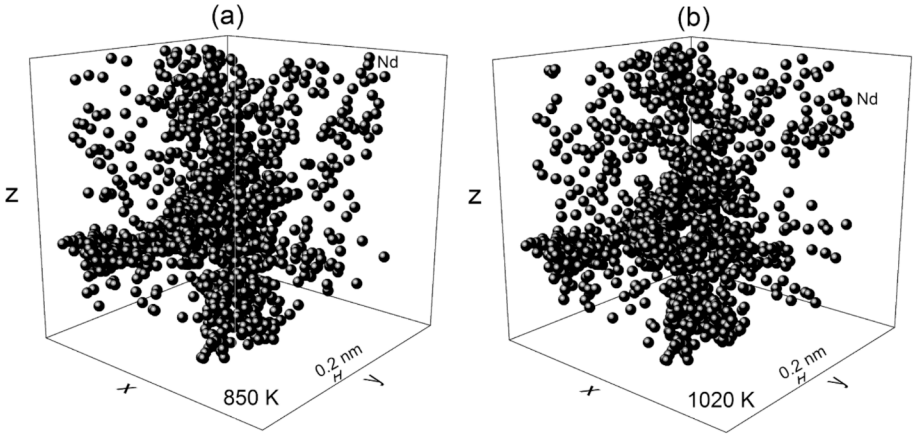

Fig. 6. The placement of Nd^{3+} ions in the FLiNaK + 15 mol.% NdF_3 system at the end of the calculation at temperatures of: (a) 850 K, and (b) 1020 K.

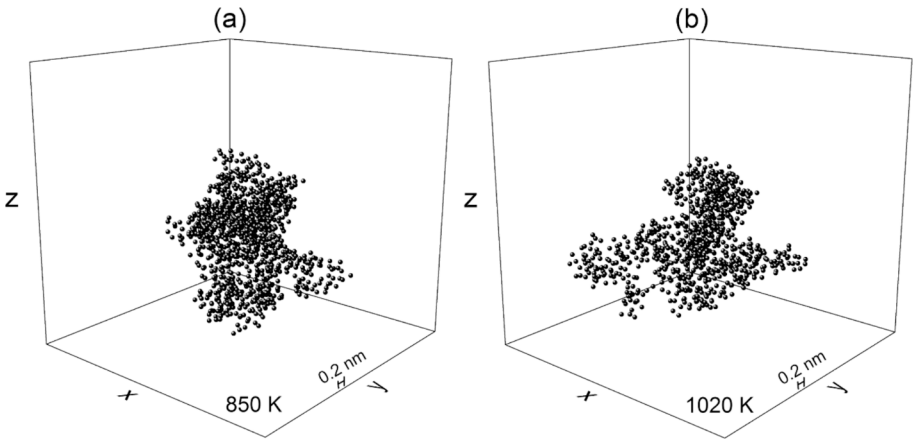

Fig. 7. Nodes of the bond network with bond lengths not exceeding 0.27 nm between the ions Nd^{3+} and F^- in the FLiNaK + 15 mol.% NdF_3 system by the end of the calculation at a temperatures: (a) 850 K and (b) 1020 K.

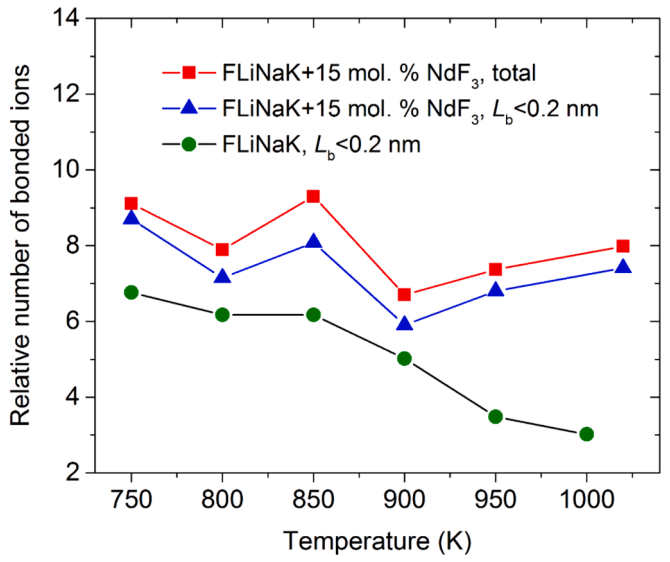

Fig. 8. The temperature dependence of the relative number of bonded ions for the systems: FLiNaK and FLiNaK + 15 mol.% NdF_3; in the legend, "total" means that the bond lengths L_b of all positive ions with F^-, which do not exceed 0.2 nm, as well as L_b of dissolved ions with Nd^{3+}-F^- bonds not exceeding 0.27 nm, are taken into account.

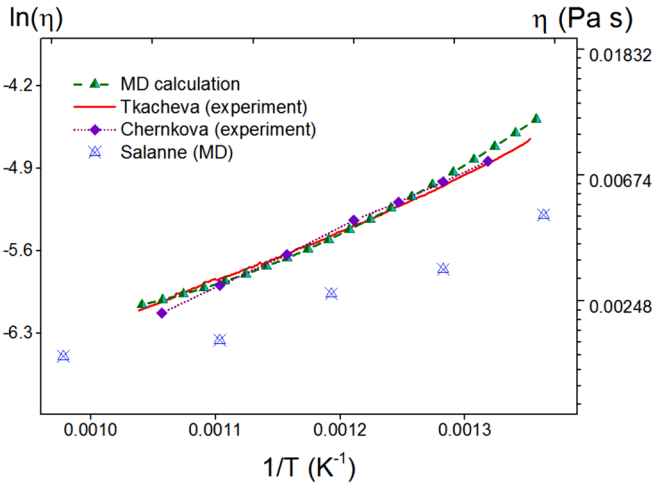

Fig. 9. Viscosity of FLiNaK melt in a semi-logarithmic scale, calculated in the current MD model (highlighted in green), compared to data obtained by various authors: Tkacheva [34], Chernkova [35], Salanne [23]. (For interpretation of the references to colour in this figure legend, the reader is referred to the web version of this article.)

viscosity of the system varies nonlinearly according to the Arrhenius equation:

$$\eta = \eta_0 \bullet exp\left(\frac{E}{RT}\right) \quad (6)$$

where η is the dynamic viscosity, η_0 is the pre-exponential factor obtained in the experiment, E is the activation energy, $R = 8.3145$ J/(mol K) is the gas constant, T is the temperature.

Fig. 9 shows the $\ln\eta\left(\frac{1}{T}\right)$ linearized data in a semi-logarithmic scale (true viscosity values are shown on the right axis) obtained by various authors in the experiments and calculated in the MD model. It can be noted that the results obtained in the current model show good agreement with the literature data.

Similarly, the temperature dependences of viscosity were calculated for the melts containing 5 and 15 mol.% of LaF_3. The results are shown in Fig. 10 together with the MD viscosity data of the pure FLiNaK system. These dependencies were obtained within the temperature range of 800 < T < 1020 K. It can be seen that the addition of 5 mol.% of LaF_3 leads to a 25 % increase in the viscosity as the temperature rises to 1020 K. Meanwhile, in the case of the 15 mol.% LaF_3 addition, the viscosity increases by more than two times compared to the pure FLiNaK melt. In the case of high concentrations of the LaF_3 additive at low temperatures (T < 850 K), the function $\eta(T)$ increases sharply reaching a value of 20 mPa·s, and the corresponding curve of $\ln\eta\left(\frac{1}{T}\right)$ deviates from the linear dependence.

For all investigated concentrations (0, 5, 15 mol. % LaF_3), the calculated temperature dependence is approximated by a function of the form $\ln\eta = a + \frac{B}{T}$, and the data are presented in Table 2.

5.3. Thermal conductivity of the FLiNaK + NdF_3 molten system

Fig. 11 shows the thermal conductivity of the pure FLiNaK melt obtained experimentally using the laser flash method [36], as well as the calculated thermal conductivity using the present MD model. In both the experimental and MD systems, a weak negative trend of thermal conductivity with temperature can be observed. We have also calculated the temperature dependence of thermal conductivity for the FLiNaK + 15 mol.% NdF_3 system, which is also presented in Fig. 11. The thermal conductivity values of the molten salt mixture containing NdF_3 increase

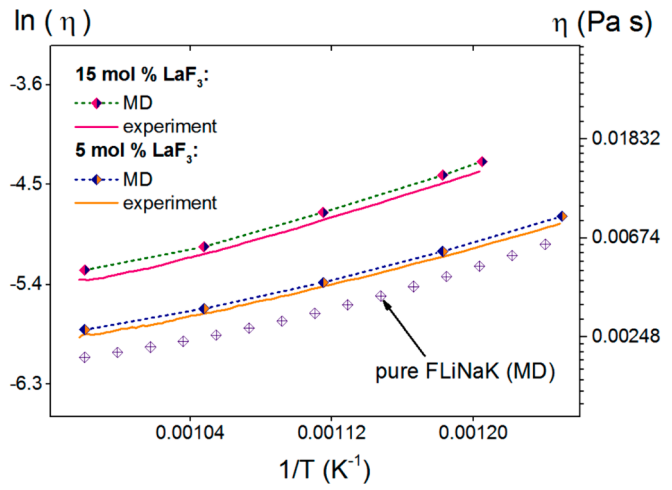

Fig. 10. The temperature dependence of viscosity (η) in semi-logarithmic scale for the FLiNaK melt, with 5 and 15 mol.% additions of LaF_3; experimental results are shown in solid line [34], while the data obtained from MD calculations are presented as points; the calculation data for the pure FLiNaK melt are also marked in the figure.

Table 2
Viscosity temperature dependences of FLiNaK + LaF_3 (C_{LaF3} = 0, 5, 15 mol. %).

LaF_3 concentration, mol. %	$f\left(\frac{1}{T}\right)$, Pa s
0	$\ln\eta = -10.58 + \frac{4490.074}{T}$
5	$\ln\eta = -9.57 + \frac{3797.96}{T}$
15	$\ln\eta = -10.61 + \frac{5344.81}{T}$

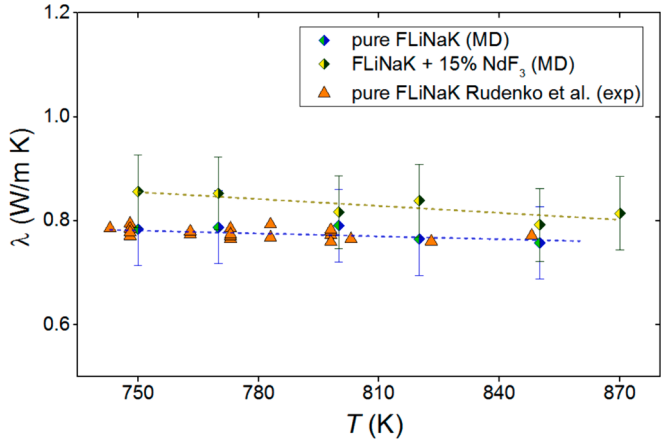

Fig. 11. Temperature dependence of the thermal conductivity of FLiNaK, and FLiNaK + 15 mol.% NdF_3 molten salts; the experimental data for pure FLiNaK obtained using the laser flash method are highlighted in orange [36]. (For interpretation of the references to colour in this figure legend, the reader is referred to the web version of this article.)

compared to the corresponding values for pure FLiNaK. In this case, a decrease in thermal conductivity with temperature is observed.

To determine the influence of density and temperature on thermal conductivity variation, we calculated the dependencies of $\lambda(\rho)$ and $\lambda(T)$ for pure FLiNaK at different average melt densities. Increasing density was achieved by raising the barostat pressure from 1 to 10,000, 15,000, and 20,000 bar. Fig. 12 illustrates the $\lambda(\rho)$ dependency at a temperature of $T = 850$ K. It can be noted that when the density changes from 1.70 to

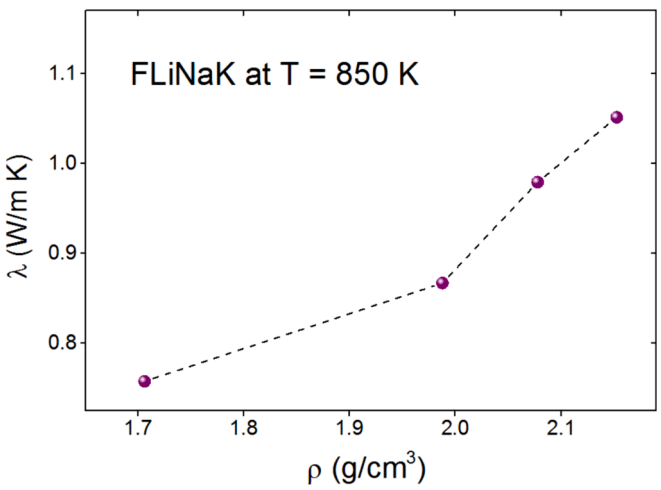

Fig. 12. The dependence of the thermal conductivity of pure FLiNaK on the melt density when the barostat pressure grows, when the temperature is constant $T = 850$ K.

2.15 g/cm^3, i.e., when the pressure increases from 1 to 20,000 bar, thermal conductivity increases rapidly (by 1.5 times).

To estimate the joint influence of density, temperature, and the addition of NdF_3 on thermal conductivity, we calculated the $\lambda(T)$ dependencies for the pure FLiNaK system (Fig. 13a) and the FLiNaK + 15 mol.% NdF_3 system (Fig. 13b) within the temperature range of $750 < T < 950$ K for different values of the average melt densities. Since the change in density at constant pressure in a given temperature range does not exceed 8 %, the figure (a) shows the average densities ρ_{avg} corresponding to various pressures of 1, 10000, 15,000 and 20000 bar in the given temperature range.

For the densities indicated in Fig. 13, the $\lambda(T)$ dependence has a weak negative trend. However, in the cases presented here, increasing pressure (average density) leads to an increasing of the $\lambda(\rho)$ by 20 %, 35 %, and 45 % for pure FLiNaK melt, and by approximately 25 % for FLiNaK + NdF_3 melt. All estimates of the thermal conductivity variation are made relative to the λ value at a standard pressure of $p = 1$ bar.

6. Discussion

This study presents a simplified model of molten salt that does not consider effects of polarization of molten salt ions, nor the lanthanide compression effect [37], when the competing filling of the 4*f* electron shell in lanthanides (and the 5*f* shell in actinides) leads to a decrease in the ionic radius of cations with rising charge.

Covalent radii are employed to denote the presence of chemical bonds and the subsequent formation of molecular structures. By utilizing covalent radii, it becomes feasible to create accurate three-dimensional representations of molecules using ball and stick models. In [38], the data of which we use, covalent radii were derived from experimental bond distances to N, C, or O. This approach seems justified, since none of these elements form a significant number of structurally characterized bonds with all elements.

According to data from [39], a chemical covalent bond between pairs of Li-F, Nd-F, and La-F atoms is formed when they approach each other at distances of 0.185, 0.258, and 0.264 nm, respectively. Similarly, Na-F and K-F chemical bonds are established at distances of 0.223 and 0.260 nm, respectively. Since among monovalent ions, the most probable and stable virtual (non-chemical) bonds in the model occur solely between Li^+ and F^-, the threshold distance for determining ion connectivity should be shorter than the length of the Na-F chemical bond, specifically 0.223 nm. In addition, since an actual Li-F chemical bond is not formed in the model, the threshold distance for identifying an interionic bond must exceed the length of the Li-F chemical bond (0.185 nm). A

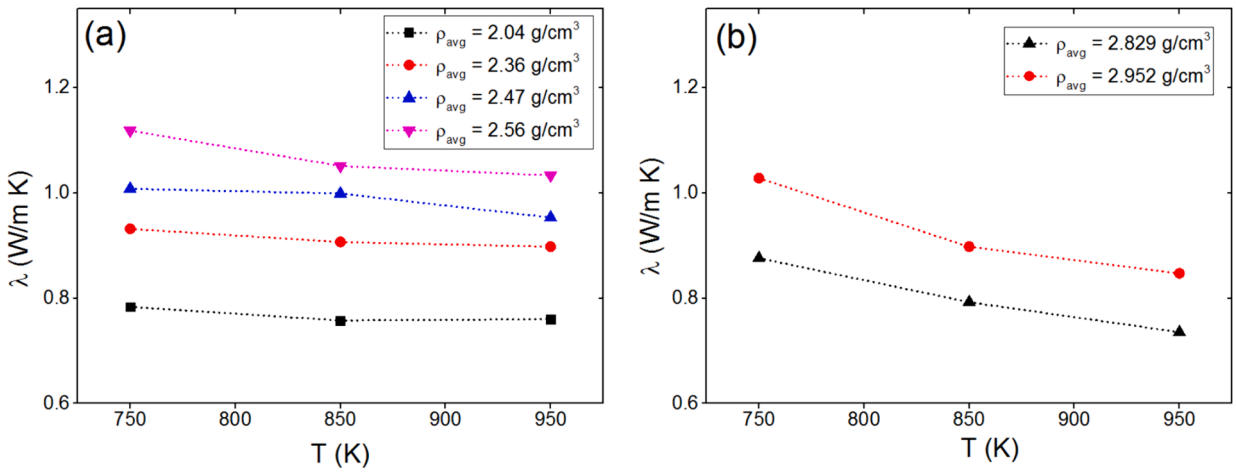

Fig. 13. The temperature dependence of thermal conductivity for different average melt densities ρ_{avg} in the systems: (a) pure FLiNaK, (b) FLiNaK + 15 mol.% NdF_3.

threshold distance of 0.2 nm satisfies both of the above requirements. At the same time, to identify the virtual Nd-F and La-F bonds in the model, the threshold distance must be greater than 0.258 and 0.264 nm, respectively.

By utilizing Slater Orbitals, quantum mechanical calculations were employed to establish absolute radii, i.e., the radii of isolated atoms, for 103 elements [40]. The determined radii for La, Nd and F are 0.08333, 0.12976 and 0.26 nm, respectively. It is the sizes of isolated atoms that should be incorporated in expressions predicting chemical bonding parameters employing the concept of the Golden ratio.

From mathematics, we are familiar with the rule of the Golden ratio, which states that when dividing a straight line into two unequal parts, a and b, such that the ratio of the length $(a + b)$ of the original line to a larger segment (for example, a) is the same as that of larger to smaller

$$(a + b)/a = a/b = \phi, \tag{7}$$

where $1/\phi = 0.618$ and $\phi^2 = 2.618$.

The Golden ratio has a unique significance when considering the core of the atom [39]. In the case of a covalent bond, the following relationships can be used to determine its length:

$$\begin{aligned} (+\,-): &\ 21/2\,LA - A = RA+ + RA- \\ (+\,+): &\ LA - A = \phi 2\,RA+ \\ (-\,-): &\ LA - A = \phi\,RA- \end{aligned} \tag{8}$$

here the signs "+" and "-" indicate the sign of the charge of the A atom (ion), R is the atomic radius, L is the bond length between the atoms (ions).

Using the radii of isolated atoms obtained in [40], and by applying the first of expressions (8), we find that the lengths of covalent bonds Li-F, La-F, Nd-F and threshold distance are determined as 0.2298, 0.2427, and 0.2756 nm, respectively. Although these values can be regarded as approximate. Taking into account the data from [39,40], we chose the threshold distances for La-F and Nd-F ion pairs to be 0.27 nm.

The viscosity of molten salts is highly dependent on the density of the system. Therefore, a significant rise in the density of the molten salt after introducing the LaF_3 additive leads to a substantial increase in the viscosity of the melts. This growth intensifies as the proportion of the additive increases. Since the preliminary MD calculation was carried out in the NPT ensemble, the density of the molten salt decreased when moving to a new calculation at a higher temperature and approximately constant pressure. With increasing temperature, the intensity of ion movement, and interionic distances, increased. This led to a decrease in system connectivity. At the same time, the viscosity of the molten salt also decreased.

An increase in temperature leads to an increase in the anharmonicity of collective vibrations created by all ions in the system, including ions that form a dynamic network of bonds. The weakening of the intensity of the "organized" oscillatory process affects the thermal conductivity, determined according to expression (4), which decreases with increasing temperature. Here, we only show the appearance of dynamic connectivity in molten FLiNaK. However, we do not take into account the contribution to thermal conductivity made by the electromagnetic flux arising from it. Since, the decrease in thermal conductivity of molten salt with temperature is usually very insignificant or even absent, it is possible that taking this contribution into account can change the temperature trend of thermal conductivity.

The thermal conductivity of most liquids (excluding water, aqueous solutions, and multihydroxy molecules) decreases with temperature. Moreover, the main mechanism of heat transfer is a molecular exchange. However, the scenario changes when solid particles (such as SiO_2 or Al_2O_3) are introduced into the molten salt, forming a nanofluid. The addition of Al_2O_3 nanoparticles to the molten salt revealed that the contribution to the thermal conductivity of the nanofluid primarily originates from atomic movements and interactions between atoms within the Al_2O_3 nanoparticle rather than within the base liquid [41].

Contrary to the classical concept of phonon thermal transfer, increasing the thermal conductivity temperature dependence is observed for superionic conductors such as chalcogenides, for example, Ag_2Te and Cu_2Se [42]. Near a temperature of 420 K, a structural phase transition from a low-temperature monoclinic β-phase to a high-temperature cubic α-phase occurs in the semiconductor-superionic material Ag_2Te. In the bulk α-Ag_2Te phase, the contributions of two different coolants (heat transfer mechanisms) were studied: phonons (conductive) and liquid-like mobile ions (convective). It was demonstrated that the rise in thermal conductivity with temperature was attributed to the predominance of convective thermal conductivity [42]. A computational study of the nature of thermal excitations in the Li_2S system undergoing a melting transition led to the conclusion of a significant contribution to thermal conductivity from convection [43]. Consequently, as the temperature reaches 700 K (in liquid Li_2S), this contribution increases to half of the total value, while the significance of vibrational scattering diminishes.

There is an opinion that the temperature trend of thermal conductivity (λ) primarily depends on the density of the melt [44]. However, there is also an alternative point of view. The dependence of thermal conductivity on the coordination number is found in various systems with covalent bonds. When the a-SiO, a-SiC, and a-Si films are hydrogenated, their thermal conductivity could decrease by up to 2 times [45]. It has been established that energy transfer occurs through a non-

hydrogen network of atoms. It has been experimentally shown that the speed of sound, atomic density and heat capacity cannot explain the measured decrease in thermal conductivity of thin amorphous films. Hydrogenation led to a decrease in the coordination number of basic atoms (not hydrogen) forming the film. It turned out that the coordination number can significantly change the scale of the coolant scattering length. It was concluded that disruption of basic atom connectivity is responsible for the reduction in thermal conductivity of amorphous films.

7. Conclusion

In this work, the behavior of the viscosity and thermal conductivity of FLiNaK, FLiNaK + MeF_3 (Me = La^{3+}, Nd^{3+}) melts in a wide temperature range was studied using the molecular dynamics method. It was demonstrated that the ratio between the connectivity of melts with and without the addition of NdF_3 correlates with the ratio of their viscosities and thermal conductivities throughout the considered temperature range. Another important finding is the decrease in both connectivity and coefficients λ and η of the FLiNaK and FLiNaK + 15 mol.% NdF_3 molten systems as the temperature rises, indicating a dependency of these kinetic coefficients on the ions' connectivity in the melt. Currently, the error in measuring thermal conductivity is high, resulting in uncertainty in the $\lambda(T)$ dependence.

The important mechanism of interaction in molten salts is ionic bonds. Moreover, the electric charges they carry capable of structuring the system. However, the intense movement of ions in molten salts impedes this process. This study demonstrates that in molten salt, a delicate equilibrium can be attained between the system's inclination to form bonds and their breakdown due to the strong Coulomb interaction between the ions within the formed bond and the surrounding ions. In the presence of such dynamic equilibrium in molten salt, there are short-lived bonds between ions with lifetime of tens to hundreds of picoseconds. Taking into account the presence in real melts of dipole moments formed by rapidly decaying pairs from negative and positive ions, as a result, some electromagnetic field should be formed in the melt. Provided the melt is isotropic, the resulting electromagnetic waves will propagate symmetrically, gradually attenuating. The attenuation of the wave will lead to the transfer of heat to the region where the dissipation of electromagnetic energy occurs; such a local temperature gradient will lead to the formation of a flow of matter, which will be determined, among other things, by the presence of internal friction in the melt. An increase in temperature leads to a decrease in the density of the melt and to a decrease in the number of Li^+-F^- ion pairs, forming a dynamic network of bonds. A decrease in the number of bound ion pairs in the melt is associated with a decrease in both viscosity and thermal conductivity of the melt.

Thus, the work proposes a concept for studying the processes of heat and mass transfer in ionic melts, based on constructing an idea of the dynamic network of bonds formed in this particular melt.

CRediT authorship contribution statement

Ksenia Abramova: Writing – original draft, Software, Methodology, Formal analysis, Conceptualization. **Alexander Galashev:** Writing – review & editing, Project administration, Formal analysis, Conceptualization. **Oksana Rakhmanova:** Writing – review & editing, Software, Conceptualization. **Konstantin Katin:** Formal analysis, Methodology, Software. **Mikhail Maslov:** Formal analysis, Methodology, Software.

Declaration of competing interest

The authors declare that they have no known competing financial interests or personal relationships that could have appeared to influence the work reported in this paper.

Data availability

Data will be made available on request.

Acknowledgements

This work is executed in the frame of the scientific theme of Institute of High-Temperature Electrochemistry UB RAS, number FUME-2022-0005, registration number 122020100205-5.

Appendix A. Supplementary data

Supplementary data to this article can be found online at https://doi.org/10.1016/j.molliq.2024.125154.

References

[1] S.A. Walker, M.E. Tano, A. Abou-Jaoude, O. Calvin, Depletion-driven thermochemistry of molten salt reactors: review, method, and analysis, Front, Nucl. Eng. 2 (2023) 1–17, https://doi.org/10.3389/fnuen.2023.1214727.
[2] B. Mignacca, G. Locatelli, Economics and finance of molten salt reactors, Prog. Nucl. Energy. 129 (2020) 103503, https://doi.org/10.1016/j.pnucene.2020.103503.
[3] A. Abou-Jaoude, S. Harper, G. Giudicelli, P. Balestra, S. Schunert, N. Martin, A. Lindsay, M. Tano, R. Freile, A workflow leveraging MOOSE transient multiphysics simulations to evaluate the impact of thermophysical property uncertainties on molten-salt reactors, Ann. Nucl. Energy. 163 (2021) 108546, https://doi.org/10.1016/j.anucene.2021.108546.
[4] R. Freile, M. Kimber, Influence of molten salt-(FLiNaK) thermophysical properties on a heated tube using CFD RANS turbulence modeling of an experimental testbed, EPJ Nuclear Sci. Technol. 5 (2019) 16, https://doi.org/10.1051/epjn/2019027.
[5] N. Galamba, C.A. Nieto de Costa, Thermal conductivity of molten alkali halides from equilibrium molecular dynamics simulations, J. Chem. Phys. 120 (2004) 8676–8682, https://doi.org/10.1063/1.1691735.
[6] H.O. Nam, A. Bengtson, K. Vortler, S. Saha, R. Sakidja, D. Morgan, First-principles molecular dynamics modeling of the molten fluoride salt with Cr solution, J. Nucl. Mater. 449 (2014) 148–157, https://doi.org/10.1016/j.jnucmat.2014.03.014.
[7] H. Shishido, N. Yusa, H. Hashizume, Y. Ishii, N. Ohitori, Evaluation of physical properties of the molten salt mixtures FLiNaBe for a fusion blanket system using molecular dynamics simulation, Fusion Sci. Technol. 68 (3) (2015) 669–673, https://doi.org/10.13182/FST14-975669.
[8] M.I. Ojovan, Viscous flow and the viscosity of melts and glasses, Phys. Chem. Glasses: Eur. J. Glass Sci. Technol. b. 53 (4) (2012) 143–150.
[9] S.V. Nemilov, Thermodynamic and kinetic aspects of the vitreous state, first ed., CRC Press, Boca Raton, FL, USA, 1995. Doi: 10.1201/9781351077286.
[10] J. Ambrosek, M. Anderson, K. Sridharan, T. Allen, Current status of knowledge of the fluoride salt (FLiNaK) heat transfer, Nucl. Technol. 165 (2017) 166–173, https://doi.org/10.13182/NT165-166.
[11] X.-H. An, J.-H. Cheng, H.-Q. Yin, L.-D. Xie, P. Zhang, Thermal conductivity of high temperature fluoride molten salt determined by laser flash technique, Int. J. of Heat and Mass Transf. 90 (2015) 872–877, https://doi.org/10.1016/j.ijheatmasstransfer.2015.07.042.
[12] M.V. Smirnov, V.A. Khokhlov, E.S. Filatov, Thermal conductivity of molten alkali halides and their mixtures, Electrochim. Acta. 32 (7) (1987) 1019–1026, https://doi.org/10.1016/0013-4686(87)90027-2.
[13] V.A. Khokhlov, V.V. Ignatiev, V. Afonichkin, Evaluating physical properties of molten salt reactor fluoride mixtures, J. Fluorine Chem. 130 (1) (2009) 30–37, https://doi.org/10.1016/j.jfluchem.2008.07.018.
[14] R. Gallagher, A. Birri, N. Russell, A. Phan, A. Gheribi, Investigation of the thermal conductivity of molten LiF-NaF-KF with experiments, theory, and equilibrium molecular dynamics, J. Molec. Liq. 361 (2022) 119151, https://doi.org/10.1016/j.molliq.2022.119151.
[15] G.J. Janz, R.P.T. Tomkins, Physical properties data compilations relevant to energy storage. IV. Molten salts: data on additional single and multicomponent salt systems, New York, 1981.
[16] B. Merritt, M. Seneca, B. Wright, N. Cahill, N. Petersen, A. Fleming, T. Munro, Thermal conductivity characterization of fluoride and chloride molten salts using a modified transient hot-wire needle probe, Int. J. Thermophys. 43 (2022) 149, https://doi.org/10.1007/s10765-022-03073-2.
[17] S.G. Robertson, R. Wiser, W. Yang, D. Kang, S. Choi, E. Bagiletto, M.P. Short, The curious temperature dependence of fluoride molten salt thermal conductivity, J. Appl. Phys. 131 (2022) 225102, https://doi.org/10.1063/5.0088059.
[18] P.B. Allen, J.L. Feldman, Thermal conductivity of disordered harmonic solids, Phys. Rev. b. 48 (1993) 12581, https://doi.org/10.1103/PhysRevB.48.12581.
[19] P.B. Allen, J.L. Feldman, J. Fabian, F. Wooten, Diffusons, locons and propagons: Character of atomic vibrations in amorphous Si, Phil. Mag. 79 (11–12) (1999) 1715–1731, https://doi.org/10.1080/13642819908223054.
[20] A. Einshtein, Über den einfluß der schwerkraft auf die ausbreitung des lichtes, Ann. Phys. 340 (10) (1911) 898–908, https://doi.org/10.1002/andp.19113401005.

[21] S. Melchionna, G. Ciccotti, B. Lee Holian, Hoover NPT Dynamics for system varying in shape and size, Mol. Phys. 78 (1993) 533–544, https://doi.org/10.1080/00268979300100371.
[22] M.P. Tosi, F.G. Fumi, Ionic sizes and born repulsive parameters in the NaCl-type alkali halides-II: The generalized Huggins-Mayer form, Phys. Chem. Solids. 25 (1964) 45–52, https://doi.org/10.1016/0022-3697(64)90160-X.
[23] M. Salanne, C. Simon, P. Turq, P.A. Madden, Heat-transport properties of molten fluorides: Determination from first-principle, J. Fluorine Chem. 130 (2009) 38–44, https://doi.org/10.1016/j.jfluchem.2008.07.013.
[24] A.Y. Galashev, O.R. Rakhmanova, K.A. Abramova, K.P. Katin, M.M. Maslov, O. Y. Tkacheva, A.V. Rudenko, A.A. Kataev, Y.P. Zaikov, Molecular dynamics and experimental study of the effect of CeF3 and NdF3 additives on the physical properties of FLiNaK, J. Phys. Chem. b. 127 (5) (2023) 1197–1208, https://doi.org/10.1021/acs.jpcb.2c06915.
[25] S.J.Plimpton, A. Kohlmeyer, A.P. Thompson, S.G. Moore, R. Berger, LAMMPS: Large-scale Atomic/Molecular Massively Parallel Simulator, Zenodo, September 29, 2021. Doi: 10.5281/zenodo.6386596.
[26] A. Stukowski, Visualization and analysis of atomistic simulation data with OVITO-the open visualization tool, Modell. Simul. Mater. Sci. Eng. 18 (2009) 015012. https:// doi. org/ 10. 1088/ 0965- 0393/18/1/ 015012.
[27] S. Sukenaga, T. Endo, T. Nishi, H. Yamada, K. Ohara, et al., Thermal conductivity of sodium silicate glasses and melts: Contribution of diffusive and propagative vibration modes, Front. Mater. 8 (2021) 753746, https://doi.org/10.3389/fmats.2021.753746.
[28] D.E. Holcomb, S.M. Cetiner, An overview of liquid-fluoride-salt heat transport systems, OAK RIDGE national laboratory Oak Ridge, Tennessee, 2010, pp. 37831–136283.
[29] T. Bryk, I.M. Mryglod, A comparative study of optic phonon-like excitations in liquid mixtures and molten salts, J. Mol. Liquids. 120 (1–3) (2005) 83–85, https://doi.org/10.1016/j.molliq.2004.07.041.
[30] N. Galamba, C.N. Castro, J.F. Ely, Shear viscosity of molten alkali halides from equilibrium and none equilibrium molecular-dynamics simulations, J. Chem. Phys. 122 (2005) 224501, https://doi.org/10.1063/1.1924706.
[31] K. Takase, N. Ohtori, Thermal conductivity of molten salt by MD simulation, Optimization of Calculation Conditions, Electrochemistry. 67 (1999) 581–586, https://doi.org/10.5796/electrochemistry.67.581.
[32] N. Ohtori, T. Oone, K. Takase, Thermal conductivity of molten alkali halides: temperature and density dependence, J. Chem. Phys. 130 (2009) 044505, https://doi.org/10.1063/1.3064588.
[33] Y. Ishii, K. Sato, M. Salanne, P.A. Madden, N. Ohtori, Thermal conductivity of molten alkali metal fluorides (LiF, NaF, KF) and their mixtures, J. Phys. Chem. b. 118 (2014) 3385, https://doi.org/10.1021/jp411781n.
[34] O. Tkacheva, A. Rudenko, A. Kataev, Viscosity of fluoride melts promising for molten salt nuclear reactors, Electrochem. Mater. Technol. 2 (2023) 20232024, https://doi.org/10.15826/elmattech.2023.2.024.
[35] M. Chrenkova, V. Danek, R. Vasilev, F. Silny, V. Kremenetsky, E. Polyakov, Density and viscosity of the (LiF-NaF-KF)eut-KBF4-B2O3 melts, J. Mol. Liq. 102 (102) (2003) 213–226, https://doi.org/10.1016/S0167-7322(02)00063-6.
[36] A. Rudenko, A. Redkin, E. Il'ina, S. Pershina, P. Mushnikov, Yu. Zaikov, S. Kumkov, Y. Liu, W. Shi, Thermal conductivity of FLiNaK in a molten state, Materials. 15 (2022) 5603, https://doi.org/10.3390/ma15165603.
[37] B.P. Sobolev, Lanthanum and lanthanide trifluorides: lanthanide contraction and volume of fluorine ion, Crystallography Reports. 65 (2) (2020) 175–181, https://doi.org/10.1134/S1063774520020212.
[38] B. Cordero, V. Gomes, A. Platero-Prats, M. Reves, J. Echeverria, E. Cremades, F. Barragan, S. Alvarez, Covalent radii revisited, Dalton Trans. 21 (21) (2008) 2832–2838, https://doi.org/10.1039/b801115j.
[39] R. Heyrovska, The golden ratio, ionic and atomic radii and bond lengths, Mol. Phys. 103 (6–8) (2005) 877–882, https://doi.org/10.1080/00268970412331333591.
[40] D.C. Ghosh, B. Raka, Theoretical calculation of absolute radii of atoms and ions. Part 1. The atomic radii, Int. J. Mol. Sci. 3 (2002) 87–113, https://doi.org/10.3390/i3020087.
[41] Q.Y. Liu Cui, G. Wei, X. Du, Mechanisms for thermal conduction in molten salt-based nanofluid, Int. J. Heat Mass Trans. 188 (2022) 122648, https://doi.org/10.1016/j.ijheatmasstransfer.2022.122648.
[42] B. Wu, Y. Zhou, M. Hu, Two-channel thermal transport in ordered–disordered superionic Ag2Te and its traditionally contradictory enhancement by nanotwin boundary, J. Phys. Chem. Lett. 9 (19) (2018) 5704–5709, https://doi.org/10.1021/acs.jpclett.8b02542.
[43] Y. Zhou, S. Volz, Thermal transfer in amorphous superionic Li2S, Phys. Rev. B 103 (2021) 224204, https://doi.org/10.1103/PhysRevB.103.224204.
[44] K. Takase, Y. Matsumoto, K. Sato, N. Ohtori, Thermal conductivity in molten alkali halides: Composition dependence in mixtures of (Na−K)Cl, Mol. Simul. 38 (2012) 432–436, https://doi.org/10.1080/08927022.2011.564171.
[45] I.L. Braun, S.W. King, A. Giri, J. Gaskins, M. Sato, T. Fujiseki, H. Fujiwara, P. E. Hopkins, Breaking network connectivity leads to ultralow thermal conductivities in fully dense amorphous solids, Appl. Phys. Lett. 109 (19) (2016) 191905, https://doi.org/10.1063/1.4967309.